J Neurophysiol 100: 2564–2576, 2008.
First published August 27, 2008; doi:10.1152/jn.90688.2008.

Spatial Relationships of Visuomotor Transformations in the Superior Colliculus Map

Robert A. Marino,[1,2,*] C. Kip Rodgers,[2,3,*] Ron Levy,[1,2,6] and Douglas P. Munoz[1,2,3,4,5]

[1]*Centre for Neuroscience Studies,* [2]*Canadian Institute of Health Research Group in Sensory-Motor Systems,* [3]*Departments of Physiology,* [4]*Psychology, and* [5]*Medicine, Queen's University, Kingston, Ontario; and* [6]*Division of Neurosurgery, Department of Clinical Neuroscience, Faculty of Medicine, University of Calgary, Foothills Medical Centre, Calgary, Alberta, Canada*

Submitted 17 June 2008; accepted in final form 26 August 2008

Marino RA, Rodgers CK, Levy R, Munoz DP. Spatial relationships of visuomotor transformations in the superior colliculus map. *J Neurophysiol* 100: 2564–2576, 2008. First published August 27, 2008; doi:10.1152/jn.90688.2008. The oculomotor system is well understood compared with other motor systems; however, we do not yet know the spatial details of sensory to motor transformations. This study addresses this issue by quantifying the spatial relationships between visual and motor responses in the superior colliculus (SC), a midbrain structure involved in the transformation of visual information into saccadic motor command signals. We collected extracellular single-unit recordings from 150 visual-motor (VM) and 28 motor (M) neurons in two monkeys trained to perform a nonpredictive visually guided saccade task to 110 possible target locations. Motor related discharge was greater than visual related discharge in 94% (141/150) of the VM neurons. Across the population of VM neurons, the mean locations of the peak visual and motor responses were spatially aligned. The visual response fields (RFs) were significantly smaller than and usually contained within the motor RFs. Converting RFs into the SC coordinate system significantly reduced any misalignment between peak visual and motor locations. RF size increased with increasing eccentricity in visual space but remained invariant on the SC map beyond 1 mm of the rostral pole. RF shape was significantly more symmetric in SC map coordinates compared with visual space coordinates. These results demonstrate that VM neurons specify the same location of a target stimulus in the visual field as the intended location of an upcoming saccade with minimal misalignment to downstream structures. The computational consequences of spatially transforming visual field coordinates to the SC map resulted in increased alignment and spatial symmetry during visual-sensory to saccadic-motor transformations.

INTRODUCTION

Multiple sensory and motor-related topographic maps have been identified in both cortical and subcortical regions of the brain. One benefit of these maps regardless of modality is to allow for the precise spatial localization of the sensory input signal and the appropriate motor response (Kaas 1997; Talbot and Masson 1941). Understanding how these maps encode sensory and motor information spatially and facilitate accurate sensorimotor transformations is a fundamental question in neuroscience. For example, in the oculomotor system, a visually guided saccade requires a precise eye movement to align the fovea directly onto a specific visual stimulus. It is generally assumed that this action requires a spatially precise transformation from visual-sensory to saccadic-motor commands. However, the relations between sensory and motor mappings and their interactions during sensorimotor transformations have never been systematically quantified. How these neural maps spatially represent and relay different sensorimotor transformations is important to understanding what the underlying neural mechanisms are computing and establishes a link between visual input and motor output.

The superior colliculus (SC) is an ideal structure to study these spatial transformations in the oculomotor system because it serves as a sensorimotor integration node with a well-understood topographically organized retinotopic sensorimotor map (Robinson 1972; Schiller and Koerner 1971; Sparks et al. 1976; Wurtz and Goldberg 1972) that has been defined mathematically (Ottes et al. 1986; Van Gisbergen et al. 1987) (Fig. 1*A*). Individual visuomotor (VM) neurons in the intermediate layers of the SC (SCi) contain organized response fields (RF), whereby individual neurons discharge a burst of action potentials for both saccades and the appearance of visual targets to a restricted region of the visual field (Sparks and Mays 1980; Wurtz and Goldberg 1972). The SC plays a pivotal role in integrating afferent sensory information into efferent motor signals for controlling saccadic eye movements (Hall and Moschovakis 2003; Krauzlis 2005; Munoz et al. 2000; Sparks 1986). However, the precise spatial relationships of these sensory and motor signals within the SC map have not been described and are fundamental to understanding sensorimotor transformations in the oculomotor system.

In this study, we quantify visuomotor transformations in the SCi to better understand the computational consequences of representing these signals within an organized spatial map. These computational consequences determine how sensory to motor transformations are simplified, or spatial discrepancy is reduced by transforming signals into SC space (Fig. 1*A*). Previous studies exploring spatial sensorimotor activity in the SC exhibit two major limitations: *1*) neural responses to sensory or motor activity was only assessed from a limited spatial density of target locations (Anderson et al. 1998; Goldberg and Wurtz 1972; Sparks et al. 1976) or along a single dimension of possible locations (Munoz and Wurtz 1995b) and *2*) predictability of target location or time of target appearance elicited preparatory activity which can contaminate the pure sensorimotor responses (Basso and Wurtz 1997, 1998; Dorris and Munoz 1998; Munoz and Wurtz 1995a). Here we avoided these limitations by employing a visually guided saccade task

* R. A. Marino and C. K. Rodgers contributed equally to this work.
Address for reprint requests and other correspondence: D. P. Munoz, Centre for Neuroscience Studies, Queen's University, Kingston, Ontario K7L 3N6, Canada (E-mail: doug_munoz@biomed.queensu.ca).

The costs of publication of this article were defrayed in part by the payment of page charges. The article must therefore be hereby marked "*advertisement*" in accordance with 18 U.S.C. Section 1734 solely to indicate this fact.

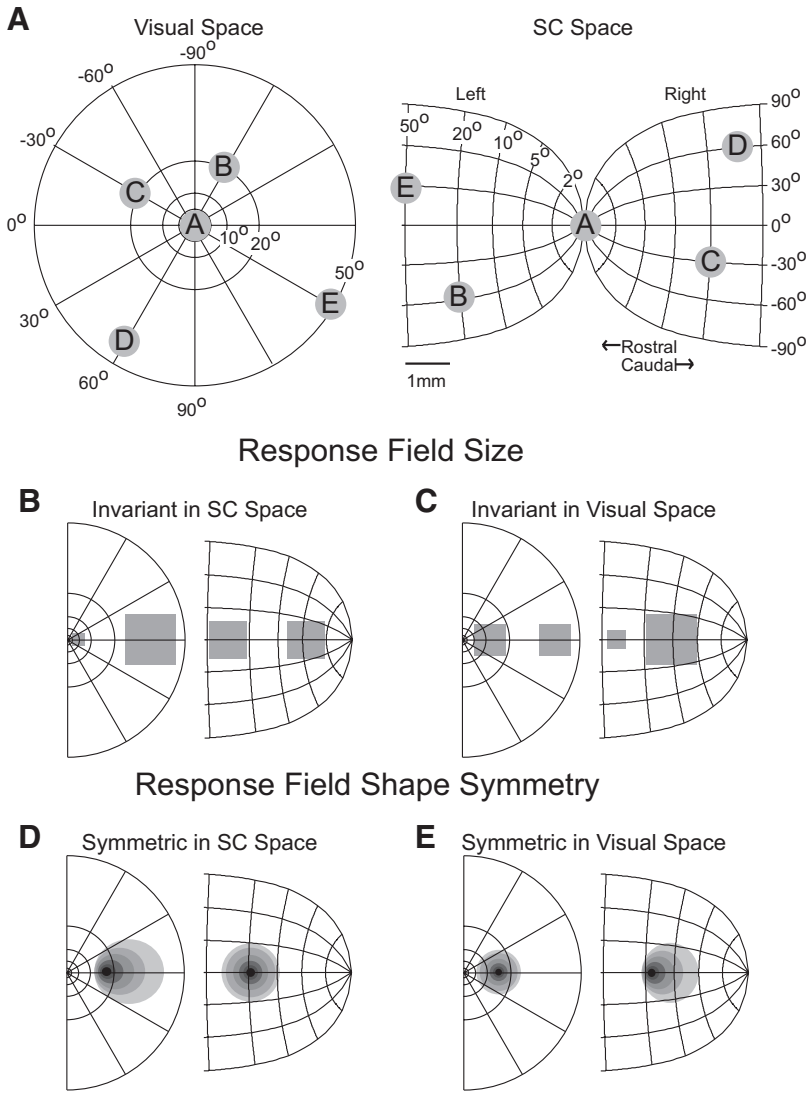

FIG. 1. *A*: logarithmic spatial transformation from visual field space to the topographic superior colliculus (SC) map using the transformations defined by *Eqs. 1* and *2* (Ottes et al. 1986; Van Gisbergen et al. 1987). *B* and *C*: potential field size relationships between target eccentricity (relative to fovea position) and receptive field (RF) size across visual and SC space. *B*: as RF eccentricity increases, RF size increases in visual space but remains invariant in SC space. *C*: as RF eccentricity increases, RF size decreases in SC space but remains invariant in visual space. *D* and *E*: potential relationships between RF shape across visual and SC space. RF shape is symmetrical in SC space and asymmetrical in visual space (*D*) or RF shape is asymmetrical in SC space and symmetrical in visual space (*E*).

with high spatial resolution that minimizes spatial and temporal prediction.

One corollary to the logarithmic mapping function between visual and SC space is that if RF size is invariant in one space, then it must change with eccentricity in the other (Fig. 1, *B* and *C*). The size and extent of population activity in the SC is an important signal parameter believed to represent a spatially weighted average of the underlying activity in the SC map coding both the visual target (Anderson et al. 1998) and saccade vector (Lee et al. 1988; Sparks et al. 1976; Trappenberg et al. 2001) locations. Thus the spatial change of visual and motor signals over the SC map can have computational consequences that include an increased recruitment of neural tissue to represent larger areas of the map. If any systematic invariance exists, then either: RF size will remain constant across SC space (McIlwain 1986; Munoz and Wurtz 1995a) and increase with increasing eccentricity across visual space (Fig. 1*B*), or RF size will decrease with increasing eccentricity across SC space and remain constant across visual space (Fig. 1*C*).

Because of the logarithmic transformation between visual and SC space (Ottes et al. 1986; Van Gisbergen et al. 1987), most spatial models assume that the underlying circuitry is evenly distributed (Fig. 1*B*) and symmetrical (Fig. 1*D*) across the SC map (Arai et al. 1994; Gancarz and Grossberg 1999; Optican 1995; Short and Enderle 2001; Trappenberg et al. 2001). In these models, the symmetrical and evenly distributed circuitry represents visual and motor activity identically and uniformly across the map. Visual to motor transformations are therefore simplified in these models because they are computing signals of the same shape and size everywhere in the map. However, this simplified view has been challenged (Nakahara et al. 2006) by suggesting that if the underlying circuitry is asymmetric in the SC (Fig. 1*E*), then the activity would inherently exhibit previously observed caudal-to-rostral (Munoz and Wurtz 1995b; Munoz et al. 1991) and lateral (Anderson et al. 1998) spread during execution of gaze shifts. As this spread has been observed physiologically and interpreted controversially as being related to gaze control (Guitton 1992; Guitton et al. 2003; Munoz et al. 1991; Wurtz and Optican 1994), it is important to assess whether RF symmetry could account for it and whether simple uniform and symmetric models of the SC should be revised.

Because VM neurons project to premotor circuitry in the brain stem reticular formation (Kato et al. 2006; Rodgers et al. 2006; Scudder et al. 1996) and are thought to shape oculomotor

(Dorris et al. 1997, 2007) and head motor commands (Corneil et al. 2004), understanding the visuo-motor transformation in the SC is a critical link between sensory input and motor output. The specific aims of this study are to assess the computational consequences of spatially transforming sensorimotor activity from visual space into SC space by determining the spatial correspondence between visual and motor RFs in visual and SC space, testing whether RF size is invariant across either visual or SC space (Fig. 1, *B* and *C*), and testing whether RF shape is symmetric across either visual or SC space (Fig. 1, *D* and *E*).

Our data reveal a tight spatial alignment between visual- and motor-related information within the intermediate layer of the SC and show that transforming activity into SC coordinates improves alignment between sensory and motor signals. Furthermore, transforming from visual space to SC space produces more symmetrical RFs (Fig. 1*D*) with sizes that are relatively invariant across eccentricity (Fig. 1*B*).

METHODS

Animal preparation

All animal care and experimental procedures were in accordance with the Canadian Council on Animal Care policies on the use of laboratory animals and approved by the Queen's University Animal Care Committee. Two male monkeys (*Macaca mulata,* 4 and 12 kg) were trained to perform oculomotor tasks. The evening prior to surgery, the animal was placed under Nil per Os (NPO, water ad lib), and a prophylactic treatment of antibiotics was initiated [5.0 mg/kg enrofloxacin (Baytril)]. On the day of the surgery, anesthesia was induced by ketamine (6.7 mg/kg im). A catheter was placed intravenously to deliver fluids (lactated Ringer) at a rate of 10 $ml \cdot kg^{-1} \cdot h^{-1}$ to a maximum of 60 ml/kg throughout the duration of the surgical procedure. Glycopyrolate (0.013 mg/kg im) was administered to control salivation, bronchial secretions, and to optimize heart rate (HR). An initial dose was delivered at the start of surgery followed by a second dose 4 h into the surgery. General anesthesia was maintained with gaseous isofluorene (2–2.5%) after an endotracheal tube was inserted (under sedation) induced by an intravenous bolus of propofol (2.5 mg/kg). HR, pulse, pulse oximetry saturation (SpO_2), respiration rate, fluid levels, circulation, and temperature were monitored throughout the surgical procedure.

To allow access of microelectrodes to the SC, a craniotomy was made based on stereotaxic coordinates of the SC, centered on the midline and angled 38° posterior of vertical. The stereotaxic apparatus (KOPF Instruments) stabilized the animal's head during implantation of stainless steel screws, which served to anchor the explant (recording chambers and head post stabilized with acrylic cement) to the skull. A stainless steel recording chamber (Crist Instruments) allowed for mounting of a microdrive, and a stainless steel head holder was embedded in the acrylic explant. The chamber was tilted 38° posterior to vertical to allow for access to the SC. Sterilized scleral search coils (19–20 mm diam) were inserted subconjunctivally into each eye (Judge et al. 1980) and were used to measure eye position with the search coil technique (Robinson 1963). The search coil leads had a Powell connector attached at termination that was embedded in the acrylic explant. The analgesic buprenorphine (0.01–0.02 mg/kg im) was administered throughout the surgery and during recovery (8–12 h). The antiinflammatory agent ketoprofen (2.0 mg/kg 1st dose, 1.0 mg/kg additional doses) was administered at the end of the surgery (prior to arousal), the day after the surgery, and every day thereafter (as required). Monkeys were given ≥2 wk to recover prior to onset of behavioral training.

Behavioral paradigms

Behavioral paradigms and visual displays were under the control of two Dell 8100 computers running UNIX-based real-time data control and presentation systems (Rex 6.1) (Hays et al. 1982). Monkeys were seated in a primate chair with their heads restrained for the duration of an experiment (2–4 h). They faced a display cathode ray tube monitor that provided an unobstructed view of the central visual area 54 × 44°. For this study, each monkey was required to perform a visually guided saccade task (Fig. 2*A*). Experiments were performed in total darkness with individual trials lasting ~1–2 s. Each trial required a single saccade to a specific visual target located some distance away from the central fixation point. The display screen was diffusely illuminated during the inter-trial interval (800–1,500 ms) to prevent dark adaptation. At the start of each trial, the screen turned black and, after a period of 250 ms, a central fixation point (0.5° diameter spot, $25 cd/m^2$) appeared at the center of the screen. The monkeys had 1,000 ms to initiate fixation, and they were required to maintain fixation for 300–500 ms. Following fixation, the fixation point was extinguished and a visual target (0.5° diam spot, $25 cd/m^2$) was presented simultaneously in the periphery. The monkeys had 500 ms to initiate a saccade to the target and were required to fixate on the target for an additional 300 ms. Each correct trial was rewarded with a drop of fruit juice or water. Luminance was measured with an optometer (UDT instruments, model S471) that was positioned directly against the screen of the monitor and centered on the stimulus. Targets were presented along one of 12 directions at amplitudes of 1, 2, 4, 6, 9, 12, 16, 20, 25, or 30° from central fixation (Fig. 2*B*). Purely vertical saccades could not be tested beyond the 20° locations and purely horizontal saccades could not be tested beyond 25° due to the shape of the monitor. This gave a total of 110 possible target locations that were randomly interleaved.

Recording techniques

Extracellular recording was performed with tungsten microelectrodes (0.5–5 MΩ impedance, Frederick Haer) inserted through guide tubes (23 gauge) that were anchored in delrin grids with 1-mm hole separations inside the recording chamber (Crist et al. 1988). Electrodes were advanced with a microdrive to the dorsal surface on the SC, distinguished clearly by large increases in multiunit activity following each saccade or change in visual stimuli. The electrodes were then lowered ~1,000 μm into the intermediate layers of the SC to a location with saccade-related activity, and we proceeded to isolate single neurons.

Data collection

Multi-unit waveforms (800 μs, sampled at 40 kHz) were triggered in real-time from amplified and filtered (150 Hz to 9 kHz) neural activity recorded with Plexon data acquisition hardware (Plexon). Neural and behavioral data were viewed on-line with commercially available software (Sort Client 2.1, Plexon) that made it possible to isolate single or multiple neurons from an individual electrode. Confirmation of accurate isolation and modifications to neural sorting was performed off-line (off-line sorter 2.5, Plexon). Horizontal and vertical eye position was collected from one eye and sampled at 1 kHz. The precise onset and end of each saccadic eye movement was identified off-line. Figure 2*C* illustrates the saccadic reaction time (SRT: the time from target appearance to saccade initiation) distribution of correct saccades collapsed across all 110 target locations from both monkeys. The shape of the distribution indicated a single modal skewed normal distribution (mean: 166 ms) that is characteristic of SRT distributions (Carpenter and Williams 1995). Trials with SRTs of <120 ms (11.7% of all trials) were excluded from analysis to remove anticipatory responses (saccades made before target perception) and express saccades (in which visual and motor related discharges over-

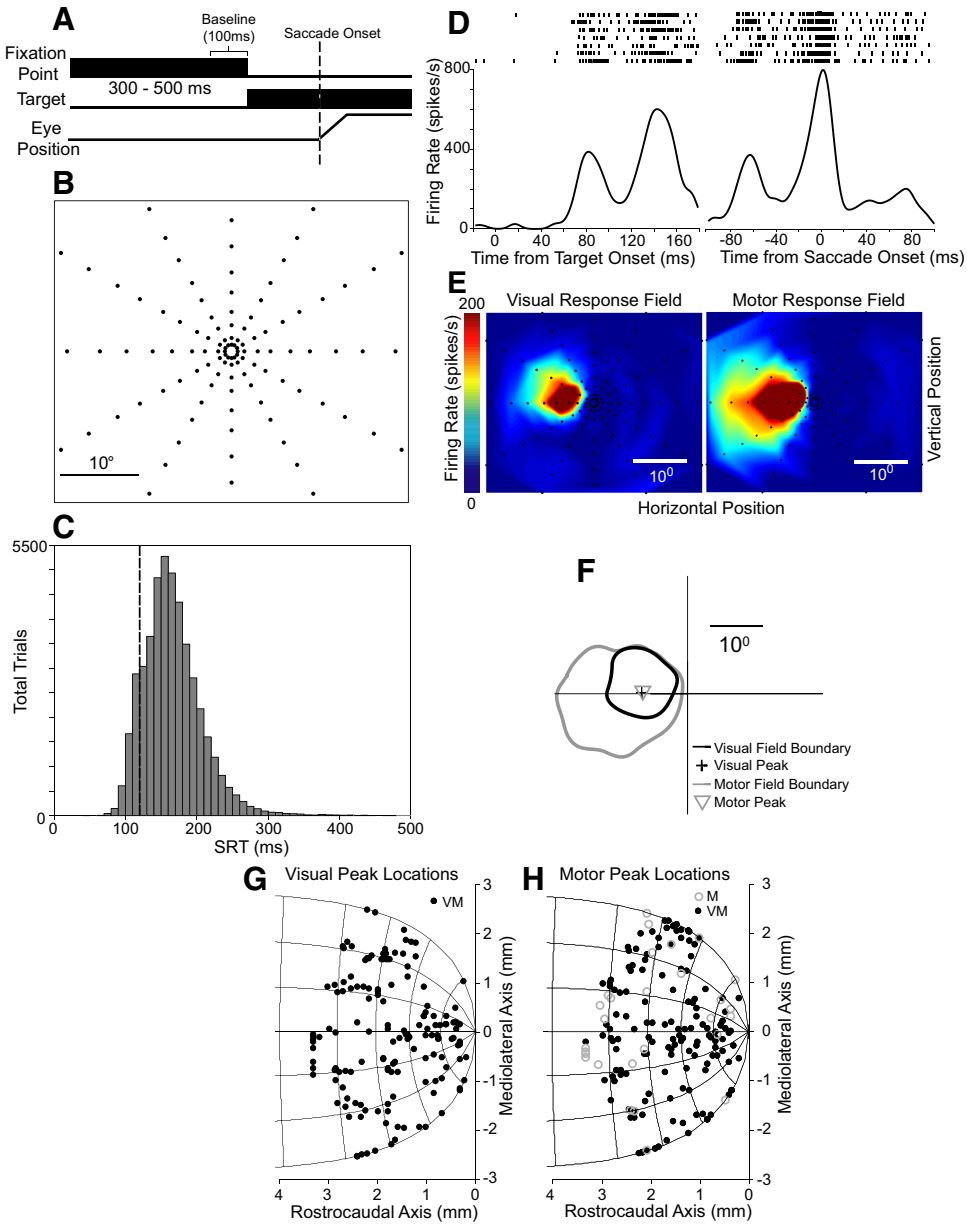

FIG. 2. *A*: schematic representation of the visually guided saccade task used in this study. Baseline activity was calculated from the last 100 ms of fixation before the appearance of the target. *B*: 110 target locations (black circles) presented at 12 different directions and 8–10 different eccentricities. *C*: saccadic reaction time (SRT) distribution histogram for all saccades (n = 45,633 trials). Vertical dashed line, the 120-ms cutoff time whereby early anticipatory responses and express saccades were removed (11.7% of all trials were removed). *D*: rasters and spike density function of a representative visual-motor (VM) neuron for target-aligned (*left*) and saccade-aligned (*right*) responses to the optimal target location, 9° along the horizontal meridian in the left visual hemifield. *E*: visual (*left*) and motor (*right*) RFs for representative neuron shown in *D*. *F*: visual and motor RF boundaries defining area with activity 3 SD above baseline for representative neuron shown in *D* and *E*. + and ▲, visual and motor peak response vectors calculated from the location of maximal activity in *E*. *G* and *H*: neuron locations on the SC map. The anatomical location of each neuron recorded was determined by the spatial location of its peak visual response (*G*) and peak motor response (*H*) converted onto the SC map. Black closed circles and gray open circles, VM and motor (M) neurons, respectively.

lap) (Dorris et al. 1997; Edelman and Keller 1996; Sparks et al. 2000) from further analysis. This ensured that visual responses were analyzed separately from motor-related activity. This was confirmed by the timing of the peak visual responses of all VM neurons, which occurred with latencies between 70 and 100 ms after target appearance. The distinct separation of visual and motor activity was also confirmed within each VM neuron by the experimenter during off-line analysis.

Average spike density functions and neuron classification

Neuron activity associated with target locations that had four or more repeated trials to each of the 110 possible target locations were included in the analysis. Trains of action potentials for each trial were convolved into spike density functions using a Gaussian kernel (σ = 5 ms) for each spike. Spike density functions were aligned on target onset when analyzing visual responses and saccade onset when analyzing motor responses (Fig. 2*D*). Neural activity from repeated trials with the same target location were summed together and averaged to produce a spike density function of a neuron's visual and motor responses to each target. Neurons were classified as either VM or motor (M) based on the presence of saccadic motor with or without visual sensory-related activity, respectively. A significant visual response was classified based on an increase of activity with a distinct peak of >60 spike/s during an epoch of >60 ms following target presentation but prior to the onset of saccade-related activity. A significant motor response was classified based on an increase in activity >80 spike/s ±1 ms around saccade onset. Baseline activity was calculated as the average discharge from all correct trials during the last 100 ms of active central fixation prior to target appearance (Fig. 2*A*).

Calculation of individual neuron response fields and peak response vectors

For each neuron, visual-related discharge rate was calculated from target-aligned average spike density functions at ±1 ms around the time of peak visual activity occurring over a time interval of 60–100 ms following target presentation. Motor-related discharge was calcu-

lated from saccade-aligned spike density functions ±1 ms around saccade onset for saccades with SRT >120 ms. The spatial extent of the visual and motor RFs were calculated with a cubic spline (de Boore 1978) that interpolated between the 110 possible target locations across the visual field (Fig. 2*E*). Visual and motor RFs were defined spatially as the area in visual or SC space (within the viewable area of the display monitor) that contained activity >3 SD above baseline activity (e.g., Fig. 2*F*).

Data obtained in visual field coordinates were also transformed into SC coordinates based on the following transformations described by Van Gisbergen and colleagues (Ottes et al. 1986; Van Gisbergen et al. 1987)

$$u = B_u \ln\left(\frac{\sqrt{R^2 + 2AR\cos(\Phi)}}{A}\right) \quad (1)$$

$$v = B_v \arctan\left(\frac{R\sin(\Phi)}{R\cos(\Phi) + A}\right) \quad (2)$$

Where u denotes the anatomical distance from the rostral pole (mm) along the horizontal position axis, v is the distance (mm) along the vertical axis, R is the retinal eccentricy, and Φ is the meridional direction of the target (deg). The constants are $B_u = 1.4$ mm; $B_v = 1.8$ mm/rad; and $A = 3°$.

Calculation of individual neuron response field peak and asymmetry

The location of the peak response was determined from the point of maximal activity in the visual and motor RFs plotted in visual or SC space. The eccentricity of the peak activity in the visual field was defined as the distance from the peak of the visual and motor RFs to the central fixation point. The eccentricity of this peak response in SC space was defined as the distance from the peak of the visual and motor RFs to the rostral pole of the SC. We chose to measure distances in SC space linearly to be consistent and comparable with visual space. To confirm that the linear distances measured in SC space did not differ significantly from the corresponding logarithmic distances measured along the curved isolines, we compared the percent difference in eccentricity between linear and logarithmic measures (logarithmic distance/linear distance). The mean percent difference in the eccentricity of the peak visual and motor responses were 2.35 ± 0.18 and 2.26 ± 0.19% (means ± SE), respectively, across the population of 150 VM neurons when measured logarithmically rather than linearly. This difference between linear and logarithmic measures was therefore very small (2%) and did not significantly change any of the findings of this paper.

Thirteen of 150 neurons were removed from the analysis of peak visual and motor locations in SC space because they exhibited peak visual and motor responses that were nearly vertical and located on opposite sides of the vertical meridian. (This mapped the peak visual and motor responses of these neurons to opposite sides of the SC and made it impossible to compare them within the same colliculus.)

Asymmetry was defined as the distance between the location of peak visual or motor activity and the center of each neuron's RF. The center of each RF was calculated in both SC and visual space as the center of mass, where mass was assumed to be equally distributed over the entire significant area >3 SD. The normalized proportional asymmetry between visual space and SC space was determined by dividing the overall asymmetry by the mean eccentricity of the peak visual and motor responses. The 13 of 150 neurons that had peak visual and motor locations in opposite SC were eliminated from the asymmetry analysis in SC space only. Although Nakahara et al. (2006) analyzed asymmetry based on the center of mass, we utilized the center of the RF (as defined by the statistically significant spatial signal) to capture the maximal asymmetry as defined by the full extent of the shape of the RF. Because the center of mass is influenced by the peak, and the peak varied in our physiological data relative to Nakahara's modeled data, we did not want our measure of asymmetry to be artificially influenced by physiological variation in the magnitude of the peak. However, the same trends were confirmed when the asymmetry analysis was repeated using the center of mass, i.e., the correlation between asymmetry and eccentricity was reduced in the SC map relative to visual space, and overall the proportional asymmetry of the visual and motor response was significantly reduced in the SC map relative to the visual map. When computed using the center of mass, the overall measured asymmetry was reduced because the center of mass was biased closer to the peak than the center of the active area of the RF.

To determine whether the observed asymmetry was directed rostrally in visual space (Fig. 1*D*) or caudally in SC space (Fig. 1*E*), we analyzed the direction of the asymmetry for all neurons that expressed a minimum of 3% normalized asymmetry (Fig. 6*E*). We defined rostral and caudal asymmetry as any shift of the peak activity relative to the center of the RF within a direction of ±45° of either the rostral pole or the caudal SC. Unimodal Rayleigh tests were used to determine whether the distributions of the asymmetric directions were statistically unimodal relative to a uniform distribution (Baschelet 1981). This statistic is based on the mean vector length which describes similarity across a sample of angles (e.g., directions of asymmetry). For the unimodal test, a mean vector length of 0 is obtained if all angles are uniformly distributed and a value of 1 is obtained if all angles are identical. The value of a mean vector length along this continuum provides an index of unimodality that is compared with a Rayleigh distribution. The average orientation of angles in circular coordinates provides the preferred direction of a unimodal distribution.

For 99/150 of VM neurons and 19/28 of M-only neurons, the motor RFs extended beyond the outer edge of the visual display. Some of these neurons may have had unbounded (or open-ended) movement fields (Munoz and Wurtz 1995a), and some may have had a distinct distal border beyond the edge of the display. In SC space, these neurons had a peak motor response vector distal of ≥2 mm from the rostral pole. This limitation of display size indicates that some portion of the RF area was underestimated in these cells; however, this underestimation does not invalidate our results as visual RFs were found to be smaller and contained within motor RFs (Fig. 3, *A* and *B*). We would expect a theoretically perfect measure of RF area to increase the significant correlation we observed between RF area and eccentricity in visual space but would have very little impact in SC space due to logarithmic compression, which increases with distance from the rostral pole.

Our underestimation of RF area correspondingly decreased our estimation asymmetry in both SC and visual space but reduced asymmetry most significantly in visual space. As we found that asymmetry was significantly greater in visual space (Fig. 6*E*), an increase in the testable area will only magnify this finding. Furthermore, to account for observed caudal-rostral spread of activity during saccades, the asymmetry in the SC that the Nakahara model (Nakahara et al. 2006) predicted was directed toward the rostral pole. Because we have underestimated asymmetry that is directed away from the rostral pole only, our analysis of the Nakahara model's prediction is not compromised.

Calculation of neural population point image response fields and peak activity

To confirm independently the relationships between visual and motor RFs observed within individual neurons, we also analyzed the simultaneous population activity or "point images" (McIlwain 1986) of visual and motor activity across the SC in our task. The activity of all neurons was plotted simultaneously on the SC map to analyze the visual and motor-related population responses. The position of each

neuron on the SC map was determined from the location of its peak visual response (for the visual population point image, Fig. 2*G*) and peak motor response (for the motor population point image, Fig. 2*H*). An interpolation with a cubic spline fit was used to create a point image (McIlwain 1986) on the SC map. Population activity was analyzed independently using two different techniques: first by mirroring all neurons across the vertical meridians (to ensure that all neurons were plotted in the same SC) and separately by mirroring across both the horizontal and vertical meridians. Neurons were mirrored across the horizontal meridian because we found no bias in eccentricity or alignment of the visuomotor responses from the upper and lower visual field. Mirroring neurons into the same SC improved spatial resolution by exploiting the underlying symmetry of the SC map. All neurons were plotted in the left SC, while visual and motor point images were calculated for 18 different rightward saccade vectors with eccentricities ranging from 1 to 12° within ±30° visual angle from the horizontal meridian. Limiting the amplitude range to a maximum of 12° eccentricity ensured that we had sufficient neuron data points on the SC map to close the distal border of the point image within the visual range of the monitor (Fig. 2, *B, G,* and *H*). Furthermore by limiting the visual angle to ±30° from horizontal likewise ensured sufficient enough data points to close the distal border of the point image within the upper and lower vertical limits of the SC map. The population activity corresponding to each target location and saccade vector were analyzed separately. Visual and motor point image fields were defined as the area of activity >3 SD above the average baseline for the population of 150 VM neurons.

RESULTS

Discharge characteristics of single neurons

We collected complete RFs (≥4 correct trials for each of 110 target locations) from 150 VM and 28 M neurons located throughout the intermediate layers of the SCi (Fig. 2, *G* and *H*). The activity of a typical VM neuron is shown in Fig. 2*D.* This neuron had a maximal visual (351 spike/s) and motor (804 spike/s) response to its optimal target location on the horizontal meridian 9° into the contralateral visual hemifield. Figure 2*E* shows the interpolated cubic spline maps of the peak visual- and motor-related discharge, and *F* plots the 3 SD borders of the peak visual and motor RFs from the same neuron. Higher peak motor than visual related discharge was observed in 94% (141/150) of the VM neurons analyzed. The range of peak visual response latencies, calculated as the time from target appearance to the peak visual-related discharge at the peak target location, was 71–99 ms.

Spatial comparison of visual and motor response fields

Across the population, visual RFs were significantly smaller than motor RFs in both visual and SC space (Fig. 3*B*). Figure 3*A* shows the proportion of the visual RF that was contained within the motor RF for all VM neurons. In visual space, 72.7% of neurons (108 of 150) had visual RFs that were ≥90% contained within their motor RFs (Fig. 3*A,* black bars). In SC space, 80% of neurons (120 of 150) had visual RFs that were ≥90% contained within their motor RFs (Fig. 3*B,* gray bars).

Comparison of peak visual and motor response locations

The cross and triangle in Fig. 2*F* represent the peak visual (black) and motor (gray) response for the representative neuron. To compare the relative positions of the peak visual and motor response locations across the population of VM neurons, the difference between visual and motor peak locations and eccentricity was compared. There were no systematic differences in eccentricity between visual and motor peak response locations in visual space (Fig. 3*C*) and SC space (Fig. 3*E*), respectively. However, many individual neurons did exhibit some misalignment between the visual and motor peak locations as the median misalignment difference was 3.2° in visual space and 0.34 mm in SC space.

There was a significant correlation between the difference in visual and motor peak locations and eccentricity of VM neurons in both visual (Fig. 3*D,* $r = 0.58$; $P < 0.01$) and SC space (Fig. 3*F,* $r = 0.28$; $P < 0.01$); however, this correlation was significantly reduced in SC space (z-test for 2 correlations, $z = 3.14$; $P < 0.05$). That is, as the eccentricity of the peak response increased, so too did the difference between peak visual and motor response locations in both visual and SC space. However, the increasing logarithmic compression of visual space with increasing distance across SC space caused large differences between visual and motor peaks at distal target locations to be reduced.

When normalized to the mean eccentricity of the peak visual and motor response locations, the proportional percent difference between visual and motor peaks was significantly higher in visual space (49.3%) than in SC space (27.3%; Fig. 3*G,* paired t-test $P < 0.01$). This indicates that the mean misalignment between the visual and motor peaks was reduced when transformed into SC space. As a consequence, the transformation of visual signals into the SC map reduced the misalignment of sensory and motor signals.

Comparison visual and motor point images

To independently confirm the alignment of visual and motor activity in SC space, we also analyzed the simultaneous population activity or point images from all 150 VM neurons to 18 specific saccade vectors. Figure 4*A* shows an example visual (*left*) and motor (*middle*) point image from a 6° rightward horizontal saccade. The *rightmost panel* shows the boundary and peak location of each of the visual and motor responses. The visual point image was smaller and completely contained within the motor point image. The visual and motor peak locations were misaligned by 0.3 mm. Across the population of visual and motor point images to each of the 18 saccade vectors analyzed, there was no correlation between the eccentricity of the visual and motor point images and the misalignment of the visual and motor peak locations (Fig. 4*B*). Thus the misalignment of visual and motor point image peak responses did not scale with eccentricity. The visual point image was ≥95% contained within the motor point image 83% of the time when neurons were mirrored across the vertical meridian only (Fig. 4*C*). When we mirrored neurons across both the vertical and horizontal meridians, 100% of all visual point images were ≥95% contained within the motor point images. Across the population, the visual point images were smaller than the motor point images (Fig. 4*D*). Thus consistent with the single neuron data, the visual point images were smaller and tended to be contained completely within the motor point image. Figure 4*E* plots the normalized misalignment between the visual and motor point images. The normalized visuomotor misalignment of the point images (36% vert mirror; 16% vertical and horizontal mirror)

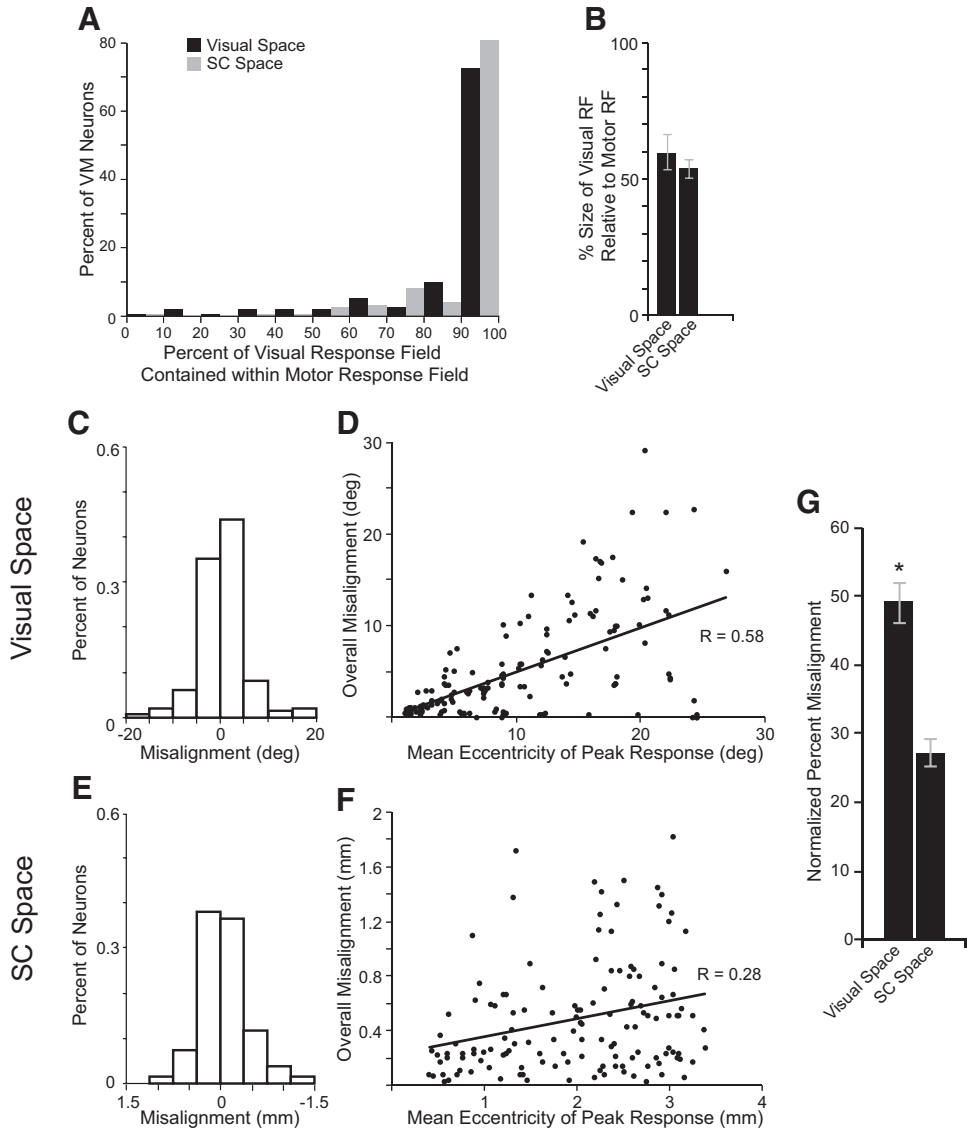

FIG. 3. Relationships between visual and motor RF areas and visual and motor peak response locations in visual and SC space. *A*: the proportion of the visual RF area that was contained within the area of the motor RF for all VM neurons ($n = 150$) in visual (■) and SC (▨) space. *B*: mean percent size of visual RF relative to motor RF across all neurons in both visual field space and SC space (visual RF area/motor RF area). *t*-test $P > 0.4$. *C*: histogram of the difference in alignment between peak visual and motor response locations in visual space. *D*: absolute difference of visual and motor peak response locations plotted against the average eccentricity of the visual and motor peak locations in degrees in visual space. —, regression line for all data points ($R = 0.58$, $m = 0.48$, $P < 0.01$). *E*: histogram of the difference in alignment between peak visual and motor response locations in SC space. *F*: the absolute difference of visual and motor peak response locations is plotted against the average eccentricity of the visual and motor peak response locations in mm on the SC map. —, regression line for all data points ($R = 0.28$, $m = 0.13$, $P < 0.01$). *G*: normalized overall proportional misalignment difference between peak visual and motor responses in both SC and visual space (overall difference/mean eccentricity of peak response) (*t*-test $P < 0.01$).

was not significantly different from the normalized misalignment calculated from the single cell analysis (27%) in SC space (*t*-test; $P > 0.05$). However, the decrease in the normalized misalignment between the vertical and the horizontal and vertical mirroring was significant (*t*-test; $P < 0.003$). This indicates that the increased data resolution gained from mirroring across both the horizontal and vertical meridians yielded visual and motor point images with reduced misalignment. Overall, the point image analysis confirmed the alignment and spatial relationships between visual and motor RFs that was independently calculated from the population of individual neurons.

Changes in response field size

To spatially assess and compare the computational consequences of representing visual and motor signals in both visual and SC space, we quantitatively assessed the relationships between RF size and eccentricity (Fig. 1, *B* and *C*). Figure 5 plots the relationships between RF size and eccentricity in visual and SC space for VM and M-only neurons. There was a strong positive correlation in visual space between the eccentricity of the peak visual response and the visual RF area for visual (Fig. 5*A*, $r = 0.51$; $P < 0.01$) and motor (Fig. 5*B*, $r = 0.65$; $P < 0.01$) responses in VM neurons. This correlation was also present among M-only (Fig. 5*B*, $r = 0.58$; $P < 0.01$). This indicates that in visual space, RF size increases with increasing eccentricity. When mapped into SC space, there was no relationship between RF area and the eccentricity of peak response vectors for visual responses in VM neurons (Fig. 5*C*, $r = 0.08$; $P > 0.3$). A significant correlation remained between motor RF area and eccentricity in SC space for the motor response of both VM (Fig. 5*D*, black line $r = 0.46$; $P < 0.01$) and M-only (Fig. 5*D*, gray line $r = 0.48$; $P < 0.01$) neurons.

Previous studies have shown that neurons located in the rostral pole of the of the SC are active during visual fixation (Munoz and Wurtz 1993) and possess very small RFs (Krauzlis 2003; Krauzlis et al. 2000; Munoz and Wurtz 1993). Antidromic identification has revealed that these neurons project more densely to the OPN region of the brain stem (Gandhi and Keller 1997). Fixation activity modulates with task epochs, and there is likely greater activation during the baseline epoch for these neurons (see Fig. 2*A*). Therefore we analyzed the popu-

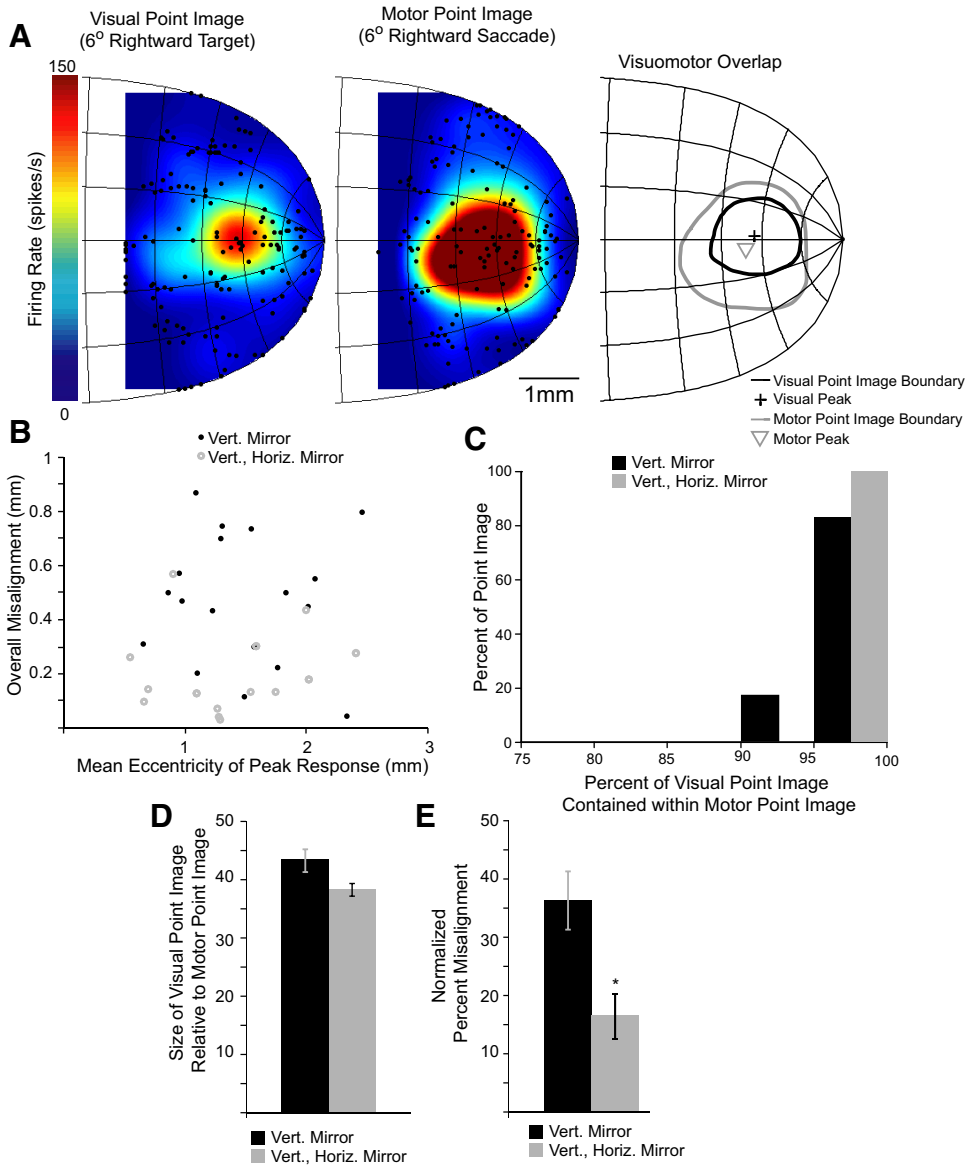

FIG. 4. *A*: simultaneous population activity (point image) from all VM cells plotted on the SC for a 6° right horizontal saccade. *Left*: the visual point image activity at the overall population peak of the visual response (90 ms after target onset). *Middle*: the motor point image activity ±1 ms around saccade onset. Each neuron is plotted on the SC map based on the spatial location of the peak visual (*left*) and motor middle response. The *rightmost panel* plots the boundary and peak of both the visual and motor point images. *B*: the absolute difference of visual and motor point image peaks is plotted against the average eccentricity of the visual and motor point image location in mm on the SC map. Black closed circles, point images in which neurons were mirrored across the vertical meridian only. Gray open circles, point image values where neurons were mirrored across both the horizontal and vertical meridians. *C*: proportion of the visual point image area that was contained within the motor point image area for 18 different saccade vectors. *D*: mean size of visual point image relative to motor point image in SC space (visual point image area/motor point image area). *E*: normalized overall proportional misalignment between peak visual and motor point images in SC space (overall misalignment/mean eccentricity of peak response) (*t*-test $P < 0.03$).

lation of neurons located <1 mm eccentricity separately. Twenty four of 150 VM and 6 of 28 M-only neurons had motor peak locations that placed them within 1 mm of the rostral pole. When neurons <1 mm were removed, the correlation between RF size and eccentricity in SC coordinates was eliminated for both VM ($r = 0.17$; $P > 0.05$) and M-only ($r = 0.09$; $P > 0.6$) populations. These data indicate that RF field size increased across the visual field with increasing eccentricity but remained invariant in SC space beyond 1 mm of the rostral pole, consistent with the hypothesis in Fig. 1*B*.

To further explore the differences between neurons within and beyond 1 mm eccentricity in SC space, we analyzed differences in baseline activity, baseline variability, and area of the motor RF (Fig. 5*E*). Both VM and M-only neurons located <1 mm of the rostral pole had significantly higher baseline activity (Fig. 5E, left) and baseline variability (Fig. 5*E, middle*) relative to those located >1 mm of the rostral pole (*t*-test; $P < 0.01$). The motor RF area of both VM and M-only neurons was also significantly smaller for neurons with peak response locations within 1 mm of the rostral pole, compared with neurons with peak response locations beyond 1 mm eccentricity (Fig. 5*E, right*). To confirm that the motor RF area <1 mm was smaller, we recalculated the area using a reduced cut off threshold of 1 SD from baseline. This reduced threshold compensated for the increased baseline variability recorded from neurons <1 mm eccentricity. With this reduced cut-off threshold, the mean motor RF area of VM neurons below 1 mm remained significantly smaller than the mean motor RF areas >1 mm (Fig. 5*E, right*). The mean motor RF area of M-only neurons also remained smaller, however the small number of M-only cells <1 mm ($n = 6$) was not enough to achieve statistical significance. (Bonferroni corrected univariate ANOVA pairwise comparisons $P < 0.05$).

Response field shape symmetry

The final goal of this study was to test whether RFs are symmetric in visual space and asymmetric in SC space (Fig. 1*D*) or asymmetric in visual space and symmetric in SC space (Fig. 1*E*) to test a specific model prediction (Nakahara et al.

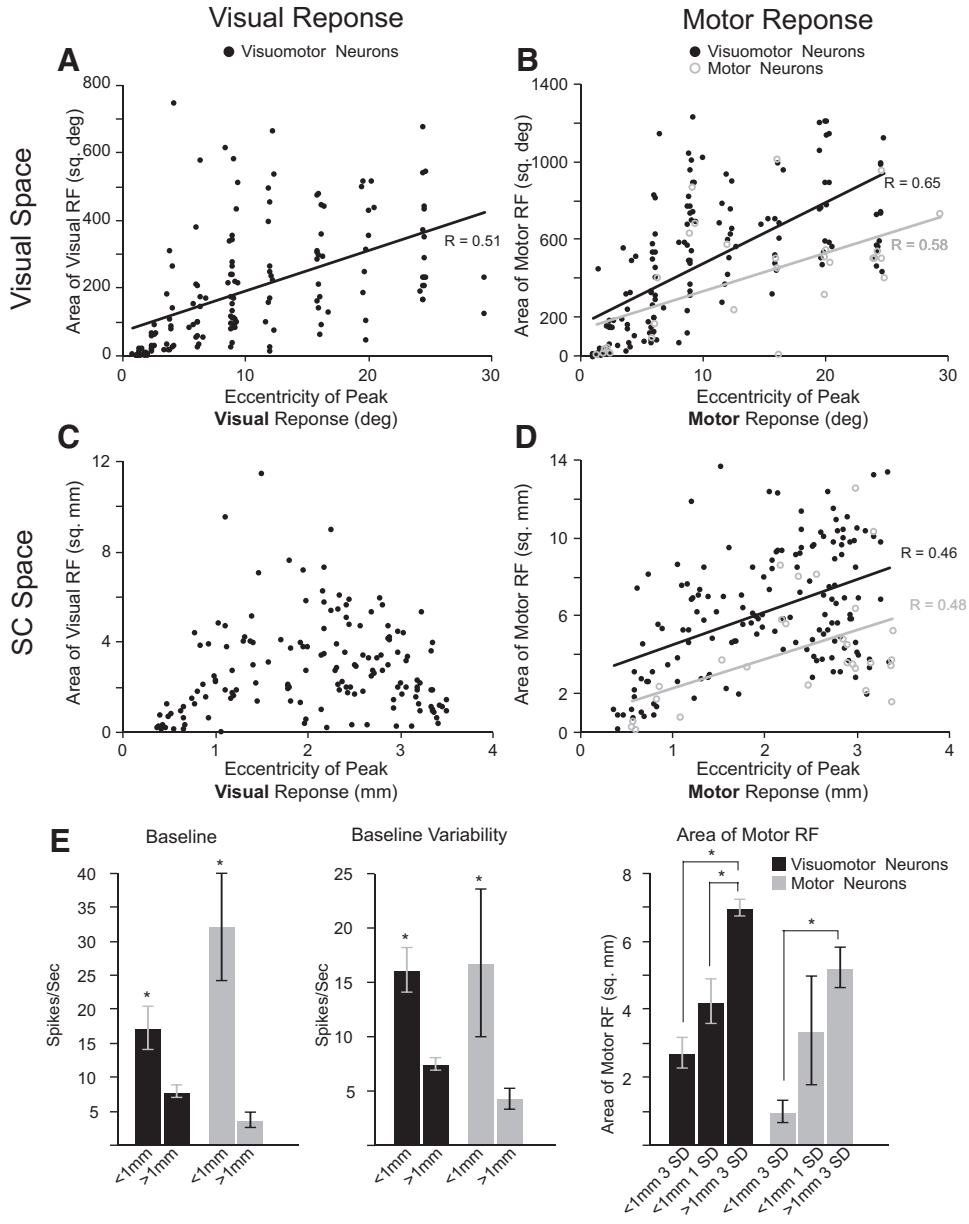

FIG. 5. Relationship between RF area and peak response eccentricity in visual space and the SC map. *A*: visual RF area of all VM neurons is plotted against the eccentricity of the peak visual response vector in visual space. —, regression line ($R = 0.51$, $m = 12$, $P < 0.01$) through all data points. *B*: motor RF area of all VM neurons (black circles) an M neurons (gray circles) plotted against the eccentricity of the peak motor response vector in visual space. Black line, regression line ($R = 0.65$, $m = 31.3$, $P < 0.01$) through VM neurons. Gray line, regression line ($R = 0.58$, $m = 19.9$, $P < 0.01$) through M neurons. *C*: visual RF area plotted against the eccentricity of the peak visual response in SC coordinates. Regression analysis was not significant for VM neurons ($R = 0.08$, $P > 0.3$). *D*: motor RF area of all VM neurons (black circles) or M neurons (gray circles) plotted against the eccentricity of the peak motor response vector in SC space. Black line, regression line ($R = 0.46$, $m = 1.7$, $P < 0.01$) through VM neurons. Gray line, regression line ($R = 0.48$, $m = 1.5$, $P = 0.01$) through M neurons. Regression analyses were not significant for VM neurons ($R = 0.17$, $P > 0.05$) or M-only neurons ($R = 0.09$, $P > 0.6$) when cells with eccentricities below 1 mm were removed. *E*: comparison of baseline activity (*left*), baseline variability (*middle*), and motor RF area (*right*) for all VM (black bars ≤ 1 mm, $n = 24$; >1 mm, $n = 126$) and M (gray bars ≤ 1 mm, $n = 6$; >1 mm, $n = 22$) neurons above and below 1 mm eccentricity on the SC map. Asterisks, statistical significance between paired means. (Bonferroni corrected univariate ANOVA pairwise comparisons $P < 0.05$.)

2006). We tested this hypothesis by comparing the symmetry of VM and M- only neuron RFs in both visual and SC space for both visual and motor responses. Figure 6 shows that there was a significant correlation between motor and visual asymmetry with increasing target eccentricity in visual (Fig. 6, *A* and *B*) and SC space (Fig. 6, C and *D*), however, this correlation was reduced in SC space for the VM visual (black, $z = 1.065$; $P < 0.15$), VM motor (black, $z = 2.58$; $^*P < 0.01$), and M-only (gray, $z = 0.8$; $P < 0.22$) populations (z-*t*est for 2 correlations). This indicates that there was some asymmetry in visual and motor RFs within both visual and SC space. When the normalized proportional asymmetry was compared, the degree of asymmetry was significantly greater (paired t-test $P < 0.01$) in visual space relative to SC space for VM visual (visual space, 49.5%, SC space, 13.8%) and motor responses (visual space, 67.6%, SC space, 26.1%) and M-only motor responses (visual space, 47.6%, SC space, 17.8%) (Fig. 6E). These data indicate that significantly greater asymmetry exists in visual field space relative to SC space (Fig. 1*D*); however, some reduced asymmetry still remains within the SC. When we analyzed the direction of the resulting asymmetry in visual and SC space for both the single cell and the population point images, we found that across all conditions there was some asymmetry directed both rostrally and caudally; however, we only found significant asymmetry in visual space biased in the rostral direction (Fig. 1*D*) for both the visual (unimodal Rayleigh test, preferred direction = 4.6° of rostral pole, $r = 0.34$, $P < 0.001$) and motor responses (unimodal Rayleigh test, preferred direction = 1.5° of rostral pole, $r = 0.43$, $P < 0.001$).

DISCUSSION

This study has shown that transformations from visual space into SC space result in several consequences that include extensive overlap between visual and motor RFs of individual neurons and population point images (Figs. 3*B* and 4*C*), reduced misalignment between peak visual and motor locations

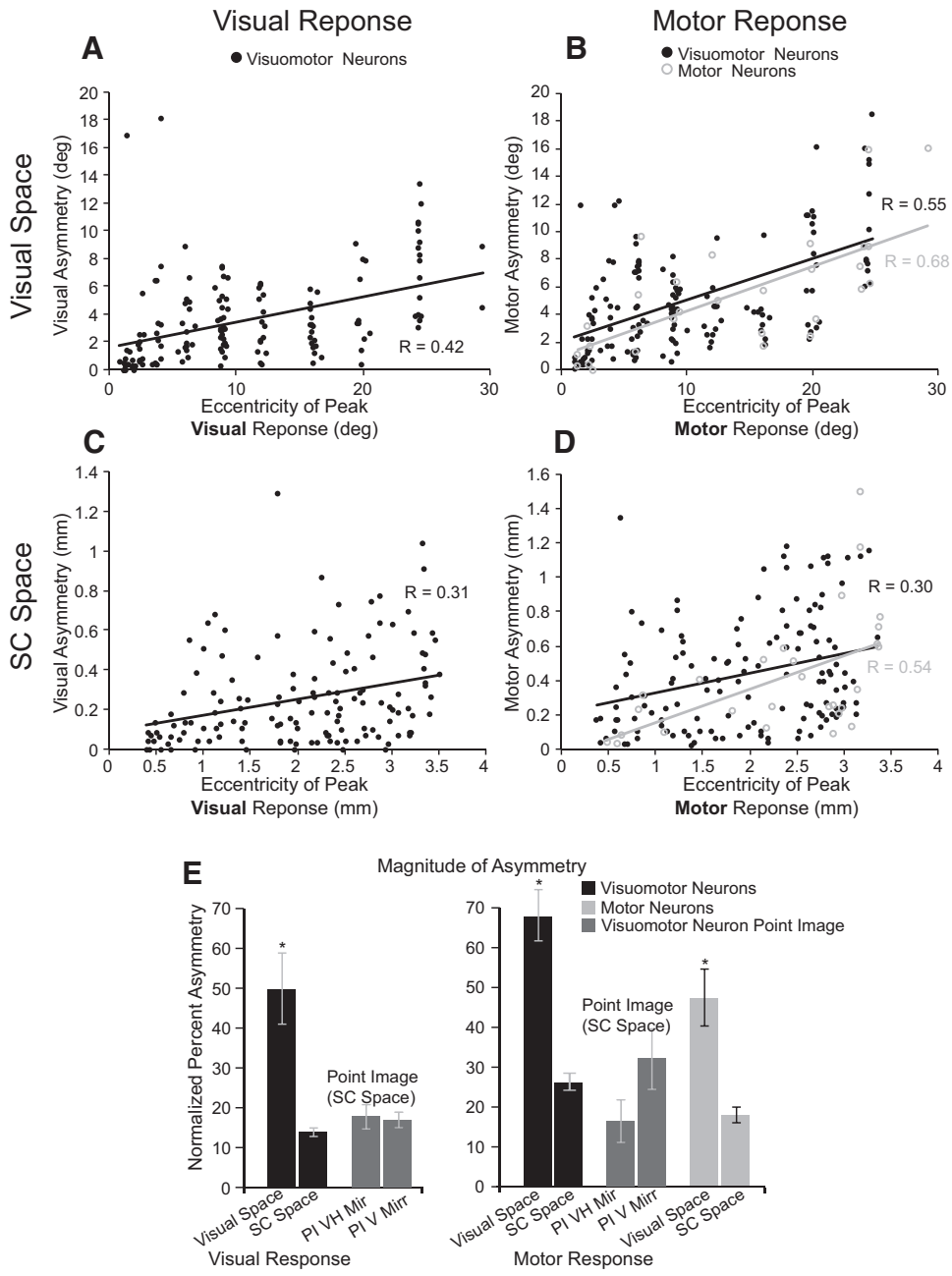

FIG. 6. Analysis of visual and motor RF asymmetry in both visual and SC space. *A*: visual asymmetry plotted against the eccentricity of the peak visual response in visual space (deg). Solid line, regression line for all data points ($n = 150$ neurons, $R = 0.42$, $m = 0.18$, $P < 0.01$). *B*: motor asymmetry (difference between motor RF peak and center locations) plotted against the eccentricity of the peak motor response in visual space (deg.). Black line, regression line ($n = 150$ neurons, $R = 0.55$, $m = 0.3$, $P < 0.01$) through VM neurons. Gray line, regression line ($n = 28$ neurons, $R = 0.68$, $m = 0.32$, $P < 0.01$) through M-only neurons. *C*: visual asymmetry (difference between visual RF peak and center locations) plotted against the eccentricity of the peak visual response in SC space (mm). Solid lin, regression line for all data points ($n = 137$, $R = 0.31$, $m = 0.08$, $P < 0.01$). *D*: motor asymmetry (difference between motor RF peak and center locations) plotted against the eccentricity of the peak motor response in SC space (mm). Black line, regression line ($n = 137$ neurons, $R = 0.3$, $m = 0.12$, $P < 0.01$) through VM neurons. Gray line, regression line ($n = 28$ neurons, $R = 0.54$, $m = 0.19$, $P < 0.01$) through M-only neurons. *E*: normalized overall proportional asymmetry (asymmetry/eccentricity of peak response) in both SC and visual space from VM neurons (black bars), M neurons (light gray bars), and population point images (dark gray bars) mirrored horizontally and vertically and vertically only. Asterisks, statistical significance between paired means (*t*-test $P < 0.05$).

(Fig. 3*G*), decreased asymmetry (Fig. 6*E*), and spatial RFs that remain size invariant over the SC beyond 1 mm (Fig. 5, *C* and *D*). Neurons located within 1 mm of the rostral pole in SC possess different discharge properties including significantly higher baseline activity (average discharge during the last 100 ms of active central fixation), higher baseline variability, and smaller RF areas (Fig. 5*E*). These findings are consistent with the discharge properties of previously recorded neurons located in the intermediate layers of the rostral SC (Krauzlis 2003; Krauzlis et al. 2000; Munoz and Wurtz 1993a, 1995a).

Spatial relationships between visual and motor response fields

There was a close alignment of the peak visual and motor vectors of VM neurons (Figs. 3, *E* and *G,* and 4*E*), confirming general assumptions that the visual and motor RFs and point images of VM neurons are aligned closely with no systematic biases. Wurtz and Goldberg (1972) reported a congruence between visual and motor RFs, commenting that they lie in the same general area but are not necessarily continuous. Sparks and colleagues (1976) noted a rough overlap but not a complete coextension of visual and motor RFs. Our results demonstrate that either visual or motor peak response vectors can be used as an accurate representation of a neuron's location on the SC map. This congruence between the location of the visual and motor responses supports previous studies that have employed either visual (Anderson et al. 1998) or motor peak response vectors (Munoz and Wurtz 1995b; Port et al. 2000; Soetedjo et al. 2002) to map visual and motor activity onto the SC.

Although neurons displayed RF areas that remained relatively constant across all locations when transformed into SC

coordinates, ~2/3 of the motor RFs had distal borders that extended beyond the area of visual space that was tested. Two caveats of this limitation are that the measurement was dependent on the statistical method used to define the boundaries of the RFs (i.e., boundary defined for discharge that were >3 SD) and that there may be an underestimation of RF size because the task was designed to test eccentricities of <30°. This underestimation, however, has a much more significant effect in visual space rather than SC space. For example, for a hypothetical neuron with a RF diameter that extends from 15 to 45° diagonally along the longest viewable target direction in the display, its diameter would be measured as 15° (to the edge of the screen), which underestimates 15° of the RF that extends beyond the 30° corner display boundary. In this hypothetical example, the RF diameter would be underestimated by 50% (15/30°) in visual space but only by 38.6% (0.53/1.37 mm) in SC space. Thus using a larger theoretical viewing area would only increase the differences in RF area and asymmetry between visual and SC space that we reported.

Alignment of peak visual and motor responses

Our data show that visual stimuli activate the same area of the SC that discharges to specify an upcoming saccade vector to that stimulus. Action potentials of VM neurons elicited by visual stimuli travel along the predorsal bundle to influence neurons in the brain stem saccade generating circuit (Kato et al. 2006; Moschovakis et al. 1990, 1996; Munoz et al. 1991; Rodgers et al. 2006). The spatial organization of the SC is conserved in projections to downstream structures in the brain stem including: rostral SC neurons projecting to omnipause neurons in the raphe interpositus nucleus (Buttner-Ennever et al. 1988, 1999), caudal SC neurons projecting to long lead burst neurons in the nucleus reticularis tegmentum pontis (Grantyn and Grantyn 1982; Scudder et al. 1996), and SC projections to the abducens nucleus (Grantyn and Berthoz 1985; Grantyn and Grantyn 1982; Olivier et al. 1993). Therefore an alignment of sensory and motor RFs among individual neurons within the SC provides oculomotor structures in the brain stem with equivocal spatial information with regard to both target and intended saccade location. This alignment of visual and motor information is likely useful for both oculomotor (Dorris et al. 1997; Edelman and Keller 1996; Sparks et al. 2000) and head premotor circuits during saccades or orienting gaze shifts that involve combined motion of the eyes and head (Corneil et al. 2004).

Spatially distinct point images resulting from confined population activity on the SC map during visually guided saccades has been demonstrated in both single-unit data (Anderson et al. 1998; Munoz and Wurtz 1995b) as well as functional imaging (Moschovakis et al. 2001). In a model of the sensory-motor transformation, McIlwain (1986) postulated that visual point images on the SC motor map shape the saccade response by "activating the appropriate combination" of output neurons. These sensory signals code the location of a stimulus that can be transformed into motor signals in the SC that are thought to specify the intended location of an upcoming saccade via vector averaging (Van Opstal and Munoz 2004). Our results indicate that such vector averaging in SC space may be simplified due to the symmetry and size invariance of visual and motor RFs. Thus theoretical vector averaging algorithms relaying desired saccade endpoints could be uniformly implemented across the SC map. This reduction in the difference between visual and motor peak locations during sensorimotor transformations in the SC acts to reduce the biological noise that may be occurring when the visual and motor peak locations do not align perfectly. Anderson and colleagues (1998) reported that a peak visual response was a more reliable measurement of a VM neuron's location in SC coordinates. Our findings support this claim as visual and motor peaks tended to be aligned (Fig. 3); visual RFs were smaller then motor RFs (Fig. 3*B*); and visual RFs tended to be entirely contained within motor RFs (Fig. 3*A*). These results suggest that VM neurons may themselves be involved in sensory-motor transformations occurring in the SC where the overlap of single-unit RFs may combine to focus population activity. As such, it would appear that the sensory RFs of SC neurons may serve to influence and possibly shape motor RFs.

Changes in response field size

An increase in RF size with increasing eccentricity was observed in visual space for both visual and motor responses with increasing eccentricity. This finding is consistent with previous studies that showed the same relationship for visual (Goldberg and Wurtz 1972; McIlwain 1986) and motor RFs (Munoz and Guitton 1991; Munoz and Wurtz 1995a; Sparks et al. 1976). When transformed into SC space, visual RFs were invariant across the SC map. Motor RFs from both VM and M-only populations were size invariant beyond 1 mm from the rostral pole, indicating that neurons within 1 mm of the rostral pole possessed different discharge characteristics related to behavior. The small RFs and increased tonic baseline activity observed in this subpopulation of cells <1 mm is consistent with these previous studies (Krauzlis et al. 2000; Munoz and Wurtz 1993a). The decreased area in SC space of neurons <1 mm indicate that these neurons have smaller RFs in SC space despite the overrepresentation of visual space at the rostral pole. However, if the modeled equations defining the SC map by Van Gisbergen and colleagues (1987) are somewhat inaccurate near the rostral pole, then neurons <1 mm could potentially maintain the same size invariance with eccentricity that was observed beyond 1 mm.

Field shape asymmetry

RF asymmetry was significantly greater in visual space relative to SC space (Fig. 6*E*) for both the single-cell and population point image data. This indicates that the underlying circuitry in SC space is more equally distributed and symmetrically connected than it would be if projected into visual space. This finding validates many previously reported SC models that were based on assumptions of symmetrical and evenly distributed connections in the SC and asymmetric connections in visual space (Arai et al. 1994; Gancarz and Grossberg 1999; Optican 1995; Short and Enderle 2001; Trappenberg et al. 2001). Nakahara's model, which is able to account for previously observed rostral spread of activity during saccades (Nakahara et al. 2006), requires asymmetrical connections in SC space that shift the peak activity caudally away from the rostral pole (Fig. 1*E*). Although our findings demonstrated significant rostrally directed asymmetry in visual

space, some reduced asymmetry was still observed in SC space (Fig. 6*E*) in both the single-cell and point image data. This reduced asymmetry in SC space was observed in both the rostral direction (where the peak activity was shifted rostral of the RF center, which occurred most often in neurons with open movement fields) and the caudal direction, but these were not significant in either the single-cell or point image population data. The observed rostrally directed asymmetry in SC space is unrelated to the caudally directed SC asymmetry that was predicted by the Nakahara model (Fig. 1*E*). Therefore it is unclear whether the remaining caudal asymmetry that was observed in SC space would be sufficient to result in the rostral spread of activity predicted by this model and previously observed physiologically (Anderson et al. 1998; Guitton and Munoz 1991; Munoz and Guitton 1991; Munoz and Wurtz 1995b; Munoz et al. 1991). Although these physiological data provide primarily contrary evidence against the Nakahara et al. (2006) model, it is important to acknowledge that the behavior in this model is primarily dependent on the lateral connection field intrinsic to the local circuitry because only a simple circular input was used. The RFs that we recorded were shaped by a combination of intrinsic lateral connections as well as external inputs that originate from many cortical and subcortical areas. However, as previous physiological evidence for a rostral spreading of activity during saccades has also been recorded in the SC in vivo where all these external inputs were active (Guitton 1992; Guitton et al. 2003; Munoz et al. 1991; Wurtz and Optican 1994), it is unlikely (based on the current evidence) that the asymmetric connections proposed by Nakahara et al. are solely responsible for this spread. These results lead to some important questions for future study. How strongly does SC input shape the resulting visual and motor activity across the map? Perhaps future studies of the isolated SC local circuit in vitro may be useful to examine RF and point image shape in isolation of external input signals. Does the shape of the RF and point image change dynamically over time course of the visual response, or the saccadic movement? Because this study only examined motor activity at saccade onset and visual activity at the time of the peak, it may be important to examine how spatial SC activity changes dynamically. It is possible that the shape of the external inputs or the local interactions within the SC map could change at different times during the visual response or the movement and result in better fits to the Nakahara et al. (2006) model.

Conclusions

Transforming visual to motor activity in SC space resulted in the following computational consequences: *1*) increased RF overlap and decreased differences between visual and motor peak locations thereby simplifying vector averaging and spatial sensorimotor transformations; and *2*) increased RF symmetry resulting in symmetrical point images across the SC map beyond 1 mm such that the area of tissue integrated over remains the same for all target vectors. Our data demonstrate that there is a close alignment of visual and motor RFs and point images in VM neurons in the SCi. Accordingly, during sensorimotor transformations in the SC, we suggest that the spatial component of an efferent SC signal is preserved and downstream structures receive equivocal information as to target location and the intended location for an upcoming saccade. Furthermore, our data support the use of both visual and motor peak vector locations in future studies to define a neuron's peak response vector as well as its subsequent position coordinates on the mathematical SC map.

ACKNOWLEDGMENTS

We thank A. Lablans, R. Pengelly, S. Hickman, and F. Paquin for outstanding technical assistance.

GRANTS

This research was supported by the Canadian Institute of Health Research. C. K. Rodgers was supported by a National Science and Engineering Council of Canada studentship, and D. P. Munoz was supported by the Canada Research Chairs Program.

REFERENCES

Anderson RW, Keller EL, Gandhi NJ, Das S. Two-dimensional saccade-related population activity in superior colliculus in monkey. *J Neurophysiol* 80: 798–817, 1998.

Arai K, Keller EL, Edelman JA. Two-dimensional neural network model of the primate saccadic system. *Neural Network* 7: 1115–1135, 1994.

Basso MA, Wurtz RH. Modulation of neuronal activity by target uncertainty. *Nature* 389: 66–69, 1997.

Basso MA, Wurtz RH. Modulation of neuronal activity in superior colliculus by changes in target probability. *J Neurosci* 18: 7519–7534, 1998.

Batschelet E. *Circular Statistics in Biology.* New York: Academic, 1981.

Buttner-Ennever JA, Cohen B, Pause M, Fries W. Raphe nucleus of the pons containing omnipause neurons of the oculomotor system in the monkey, and its homologue in man. *J Comp Neurol* 267: 307–321, 1988.

Buttner-Ennever JA, Horn AK, Henn V, Cohen B. Projections from the superior colliculus motor map to omnipause neurons in monkey. *J Comp Neurol* 413: 55–67, 1999.

Carpenter RH, Williams ML. Neural computation of log likelihood in control of saccadic eye movements. *Nature* 377: 59–62, 1995.

Corneil BD, Olivier E, Munoz DP. Visual responses on neck muscles reveal selective gating that prevents express saccades. *Neuron* 42: 831–841, 2004.

Crist CF, Yamasaki DSG, Komatsu H, Wurtz RH. A grid system and a microsyringe for single cell recording. *J Neurosci Methods* 26: 117–122, 1988.

de Boore C (editor). *A Practical Guide to Splines.* New York: Springer-Verlag, 1978.

Dorris MC, Munoz DP. Saccadic probability influences motor preparation signals and time to saccadic initiation. *J Neurosci* 18: 7015–7026, 1998.

Dorris MC, Olivier E, Munoz DP. Competitive integration of visual and preparatory signals in the superior colliculus during saccadic programming. *J Neurosci* 27: 5053–5062, 2007.

Dorris MC, Pare M, Munoz DP. Neuronal activity in monkey superior colliculus related to the initiation of saccadic eye movements. *J Neurosci* 17: 8566–8579, 1997.

Edelman JA, Keller EL. Activity of visuomotor burst neurons in the superior colliculus accompanying express saccades. *J Neurophysiol* 76: 908–926, 1996.

Gancarz G, Grossberg S. A neural model of saccadic eye movement control explains task-specific adaptation. *Vision Res 39:* 18: 3123–3143, 1999.

Gandhi NJ, Keller EL. Spatial distribution and discharge characteristics of superior colliculus neurons antidromically activated from the omnipause region in monkey. *J Neurophysiol* 78: 2221–2225, 1997.

Goldberg ME, Wurtz RH. Activity of superior colliculus in behaving monkey. I. Visual receptive fields of single neurons. *J Neurophysiol* 35: 542–559, 1972.

Grantyn A, Berthoz A. Burst activity of identified tecto-reticulo-spinal neurons in the alert cat. *Exp Brain Res* 57: 417–421, 1985.

Grantyn A, Grantyn R. Axonal patterns and sites of termination of cat superior colliculus neurons projecting in the tecto-bulbo-spinal tract. *Exp Brain Res* 46: 243–256, 1982.

Guitton D. Control of eye-head coordination during orienting gaze shifts. *Trends Neurosci* 15: 174–179, 1992.

Guitton D, Bergeron A, Choi WY, Matsuo S. On the feedback control of orienting gaze shifts made with eye and head movements. *Prog Brain Res* 142: 55–68, 2003.

Guitton D, Munoz DP. Control of orienting gaze shifts by the tectoreticulospinal system in the head-free cat. I. Identification, localization, and

effects of behavior on sensory responses. *J Neurophysiol* 66: 1605–1623, 1991.

Hall WC, Moschovakis AK (editors). *The Superior Colliculus: New Approaches for Studying Sensorimotor Integration.* Boca Raton, FL: CRC, 2003.

Hays A, Richmond B, Optican L. A UNIX-based multiple process system for real-time data acquisition and control. *WESCON Conf Proc* 2: 1–10, 1982.

Judge SJ, Richmond BJ, Chu FC. Implantation of magnetic search coils for measurement of eye position: an improved method. *Vision Res* 20: 535–538, 1980.

Kaas JH. Topographic maps are fundamental to sensory processing. *Brain Res Bull* 44: 107–112, 1997.

Kato R, Grantyn A, Dalezios Y, Moschovakis AK. The local loop of the saccadic system closes downstream of the superior colliculus. *Neuroscience* 143: 319–337, 2006.

Krauzlis RJ. Neuronal activity in the rostral superior colliculus related to the initiation of pursuit and saccadic eye movements. *J Neurosci* 23: 4333–4344, 2003.

Krauzlis RJ. The control of voluntary eye movements: new perspectives. *Neuroscientist* 11: 124–137, 2005.

Krauzlis RJ, Basso MA, Wurtz RH. Discharge properties of neurons in the rostral superior colliculus of the monkey during smooth-pursuit eye movements. *J Neurophysiol* 84: 876–891, 2000.

Lee C, Rohrer WH, Sparks DL. Population coding of saccadic eye movements by neurons in the superior colliculus. *Nature* 332: 357–360, 1988.

McIlwain JT. Point images in the visual system: new interest in an old idea. *Trends Neurosci* 9: 354–358, 1986.

Moschovakis AK, Gregoriou GG, Savaki HE. Functional imaging of the primate superior colliculus during saccades to visual targets. *Nat Neurosci* 4: 1026–1031, 2001.

Moschovakis AK, Scudder CA, Highstein SM. A structural basis for Hering's law: projections to extraocular motoneurons. *Science* 248: 1118–1119, 1990.

Moschovakis AK, Scudder CA, Highstein SM. The microscopic anatomy and physiology of the mammalian saccadic system. *Prog Neurobiol* 50: 133–254, 1996.

Munoz DP, Dorris MC, Pare M, Everling S. On your mark, get set: brainstem circuitry underlying saccadic initiation. *Can J Physiol Pharmacol 78:* 11: 934–944, 2000.

Munoz DP, Guitton D. Control of orienting gaze shifts by the tectoreticulospinal system in the head-free cat. II. Sustained discharges during motor preparation and fixation. *J Neurophysiol* 66: 1624–1641, 1991.

Munoz DP, Guitton D, Pelisson D. Control of orienting gaze shifts by the tectoreticulospinal system in the head-free cat. III. Spatiotemporal characteristics of phasic motor discharges. *J Neurophysiol* 66: 1642–1666, 1991.

Munoz DP, Wurtz RH. Fixation cells in monkey superior colliculus. I. Characteristics of cell discharge. *J Neurophysiol* 70: 559–575, 1993.

Munoz DP, Wurtz RH. Saccade-related activity in monkey superior colliculus. I. Characteristics of burst and buildup cells. *J Neurophysiol* 73: 2313–2333, 1995a.

Munoz DP, Wurtz RH. Saccade-related activity in monkey superior colliculus. II. Spread of activity during saccades. *J Neurophysiol* 73: 2334–2348, 1995b.

Nakahara H, Morita K, Wurtz RH, Optican LM. Saccade-related spread of activity across superior colliculus may arise from asymmetry of internal connections. *J Neurophysiol* 96: 765–774, 2006.

Olivier E, Grantyn A, Chat M, Berthoz A. The control of slow orienting eye movements by tectoreticulospinal neurons in the cat: behavior, discharge patterns and underlying connections. *Exp Brain Res* 93: 435–449, 1993.

Optican LM. A field theory of saccade generation: temporal-to-spatial transform in the superior colliculus. *Vision Res* 35: 3313–3320, 1995.

Ottes FP, Van Gisbergen JA, Eggermont JJ. Visuomotor fields of the superior colliculus: a quantitative model. *Vision Res* 26: 857–873, 1986.

Port NL, Sommer MA, Wurtz RH. Multielectrode evidence for spreading activity across the superior colliculus movement map. *J Neurophysiol 84:* 1: 344–357, 2000.

Robinson DA. A method of measuring eye movement using a scleral search coil in a magnetic field. *IEEE Trans Biomed Eng* 10: 137–145, 1963.

Robinson DA. Eye movements evoked by collicular stimulation in the alert monkey. *Vision Res* 12: 1795–1808, 1972.

Rodgers CK, Munoz DP, Scott SH, Pare M. Discharge properties of monkey tectoreticular neurons. *J Neurophysiol* 95: 3502–3511, 2006.

Schiller PH, Koerner F. Discharge characteristics of single units in superior colliculus of the alert rhesus monkey. *J Neurophysiol* 34: 920–936, 1971.

Scudder CA, Moschovakis AK, Karabelas AB, Highstein SM. Anatomy and physiology of saccadic long-lead burst neurons recorded in the alert squirrel monkey. I. Descending projections from the mesencephalon. *J Neurophysiol* 76: 332–352, 1996.

Short SJ, Enderle JD. A model of the internal control system within the superior colliculus. *Biomed Sci Instrum* 37: 349–354, 2001.

Soetedjo R, Kaneko CR, Fuchs AF. Evidence against a moving hill in the superior colliculus during saccadic eye movements in the monkey. *J Neurophysiol* 87: 2778–2789, 2002.

Sparks DL. Translation of sensory signals into commands for control of saccadic eye movements: role of primate superior colliculus. *Physiol Rev* 66: 118–171, 1986.

Sparks DL, Holland R, Guthrie BL. Size and distribution of movement fields in the monkey superior colliculus. *Brain Res* 113: 21–34, 1976.

Sparks DL, Mays LE. Movement fields of saccade-related burst neurons in the monkey superior colliculus. *Brain Res* 190: 39–50, 1980.

Sparks D, Rohrer WH, Zhang Y. The role of the superior colliculus in saccade initiation: a study of express saccades and the gap effect. *Vision Res* 40: 2763–2777, 2000.

Talbot SA, Masson ME. Physiological studies on neuronal mechanisms of visual localization and discrimination. *Am J Ophthalmol* 24: 1255–1263, 1941.

Trappenberg TP, Dorris MC, Munoz DP, Klein RM. A model of saccade initiation based on the competitive integration of exogenous and endogenous signals in the superior colliculus. *J Cogn Neurosci* 13: 256–271, 2001.

Van Gisbergen JA, Van Opstal AJ, Tax AA. Collicular ensemble coding of saccades based on vector summation. *Neuroscience* 21: 541–555, 1987.

Van Opstal AJ, Munoz DP. Auditory-visual interactions subserving primate gaze orienting. In: *Handbook of Multisensory Processes*, edited by Calvert GA, Spence C, Stein BE. Cambridge, MA.: MIT Press, 2004, p. 373–394.

Wurtz RH, Goldberg ME. Activity of superior colliculus in behaving monkey. III. Cells discharging before eye movements. *J Neurophysiol* 35: 575–586, 1972.

Wurtz RH, Optican LM. Superior colliculus cell types and models of saccade generation. *Curr Opin Neurobiol* 4: 857–861, 1994.